The intracellular parasite *Toxoplasma gondii* harbors three druggable FNT-type formate and L-lactate transporters in the plasma membrane

Received for publication, May 3, 2018, and in revised form, September 14, 2018 Published, Papers in Press, September 20, 2018, DOI 10.1074/jbc.RA118.003801

Holger Erler[‡], **Bingjian Ren**[§], **Nishith Gupta**[§1], **and Eric Beitz**[‡2]

From the [‡]*Department of Pharmaceutical and Medicinal Chemistry, Christian-Albrechts-University of Kiel, 24118 Kiel, Germany and* [§]*Department of Molecular Parasitology, Faculty of Life Sciences, Humboldt University, 10115 Berlin, Germany*

Edited by Karen G. Fleming

Toxoplasma gondii **is a globally prevalent parasitic protist. It is well-known for its ability to infect almost all nucleated vertebrate cells, which is reflected by its unique metabolic architecture. Its fast-growing tachyzoite stage catabolizes glucose via glycolysis to yield L-lactate as a major by-product that must be exported from the cell to prevent toxicity; the underlying mechanism remains to be elucidated, however. Herein, we report three formate–nitrite transporter (FNT)–type monocarboxylate/proton symporters located in the plasma membrane of the *T. gondii* tachyzoite stage. We observed that all three proteins transport both L-lactate and formate in a pH-dependent manner and are inhibited by 2-hydroxy-chromanones (a class of small synthetic molecules). We also show that these compounds pharmacologically inhibit *T. gondii* growth. Using a chemical biology approach, we identified the critical residues in the substrate-selectivity region of the parasite transporters that determine differential specificity and sensitivity toward both substrates and inhibitors. Our findings further indicate that substrate specificity in FNT family proteins from *T. gondii* has evolved such that a functional repurposing of prokaryotic-type transporters helps fulfill a critical metabolic role in a clinically important parasitic protist. In summary, we have identified and characterized the lactate transporters of *T. gondii* and have shown that compounds blocking the FNTs in this parasite can inhibit its growth, suggesting that these transporters could have utility as potential drug targets.**

Members of the microbial formate–nitrite transporter (FNT)[3] family perform central tasks in the metabolism of bacteria, where they transport monocarboxylate metabolites, such as formate ($HCOO^-$), its nitrogen analog nitrite (NOO^-), and even hydrosulfide (HS^-) (1–3). Formate is an end product of anaerobic acid fermentation in bacteria, which is consequently released via FocA (an FNT family protein) (1). Conversely, an import of formate via FocA enables hydrogen production by formate hydrogen lyase in bacteria (4). Likewise, hydrosulfide is generated by chemical reduction of sulfate in bacteria via both assimilatory and dissimilatory pathways. Hydrosulfide is toxic above a certain threshold and is discharged by yet another member of the FNT family, *i.e.* hydrosulfide channel (HSC) (3). Not least, the nitrite-transporting FNT from *Salmonella typhimurium*, NirC, which turned out to be a virulence factor, allows the pathogen to survive inside the digestive vacuole of macrophages (5). Here, uptake of host-derived nitrite by intracellular bacteria and its reduction to ammonia prevents the formation of nitric oxide and subsequent antimicrobial activation of the macrophage.

Bioinformatics and phylogenetic analyses have revealed the presence of FNTs in eukaryotes; however, their occurrence is limited to certain protozoans including *Amoeba* and *Apicomplexa* (6, 7). Only one eukaryotic FNT, *Pf*FNT from the human malaria parasite *Plasmodium falciparum*, has been characterized so far, which facilitates the efflux of lactate (6, 8). The lactate molecule is considerably larger than formate, nitrite, or hydrosulfide. To accommodate lactate, *Pf*FNT carries a wider substrate selectivity filter region than bacterial FNTs, which we termed Φ/K region because of its presence of a lysine residue in a lipophilic environment. Lactate is a key by-product of glycolysis in *Plasmodium*, and in other related parasites, such as *Toxoplasma gondii* (9–11). Earlier work has demonstrated the expression of high-affinity sugar permeases in both parasites (12, 13), which allow import of glucose (besides other hexoses) and its subsequent catabolism through glycolysis (14–16). Surprisingly, glucose import is essential for asexual growth of the acute (termed merozoite) stage in *Plasmodium* (17, 18) but dispensable for the acute (termed tachyzoite) stage of *T. gondii* (16, 18, 19). Previous works by several groups have also characterized lactate dehydrogenases in the two parasites (20, 21), which are meant to enable recycling of $NADH^+$ to NAD^+ and thus ensure a continued glycolysis. It is still unclear how tachyzoites of *T. gondii* eliminate lactate produced during intracellular replication. In other words, proteins underlying the lactate efflux remain to be identified in *T. gondii*.

This work was supported by German Research Foundation (Deutsche Forschungsgemeinschaft) Grants Be2253/7-1 (to E. B.) and GRK2046 (to N. G.). The authors declare that they have no conflicts of interest with the contents of this article.

This article contains Figs. S1–S4 and Table S1.

[1] To whom correspondence may be addressed: Philippstraße 13, House 14, 10115 Berlin, Germany. Tel.: 49-30-20936404; Fax: 49-30-20936051; E-mail: Gupta.Nishith@hu-berlin.de.

[2] To whom correspondence may be addressed: Gutenbergstraße 76, 24118 Kiel, Germany. Tel.: 49-431-8801809; Fax: 49-431-8801352; E-mail: ebeitz@pharmazie.uni-kiel.de.

[3] The abbreviations used are: FNT, formate–nitrite transporter; aa, amino acid; AQP, aquaporin; DAPI, 4′,6-diamidino-2-phenylindole; HFF, human foreskin fibroblast; MCT, monocarboxylate transporter; MMTS, methyl methanethiosulfonate; pCMBS, 4-(chloromercuri)benzenesulfonate; Φ/K, lipophilic lysine region.

This work focuses on the biochemical characterization, pharmacological inhibition, and mechanism of FNT proteins to demonstrate their physiological importance during the lytic cycle of *T. gondii* in mammalian cells.

Results

T. gondii harbors three FNTs on its surface

We started by searching the annotated genome of *T. gondii* for genes encoding putative monocarboxylate transporters. This search did not reveal the presence of MCT-type transporters (22); instead, we identified three FNT-encoding genes (ToxoDB IDs: TGGT1_209800, TGGT1_292110, and TGGT1_229170). The first one, TGGT1_209800, located on the chromosome Ib, appeared intron-less; we refer to the gene product of 412 amino acids (aa) as *Tg*FNT1 (44.3 kDa) herein. The second, TGGT1_292110, with six exons on the chromosome IX, encodes for *Tg*FNT2 with 463 aa (50.8 kDa), and the third TGGT1_229170, with five exons present on the chromosome VIII, translates into *Tg*FNT3 with 501 aa (53.3 kDa). The three *Tg*FNT proteins display typical signature motifs, *e.g.* in the L2 and L5 loop regions preceding the two half-helices, and a six-transmembrane topology with both termini facing intracellularly shared by all FNT family members (Fig. 1*A*) (23). Quite notably, however, the *Tg*FNTs harbor extended C termini that are about 115 to 225 aa longer than the previously reported FNTs. *Tg*FNT2 also contains an additional stretch of 70 aa at the N terminus. The sequences of the *Tg*FNT1–3 termini appear to be nonhomologous, whereas the protein cores, *i.e.* the transmembrane domains plus connecting loops, exhibit an overall 61–66% sequence identity and 75–78% similarity with each other. Finally, we cloned and verified their ORF sequences using the mRNA isolated from tachyzoites of *T. gondii*.

Next, we generated full-length ectopic expression constructs of *Tg*FNT1–3 carrying a hemagglutinin epitope (HA) at the respective C terminus for immunofluorescent localization in tachyzoites. The constructs were transfected into fresh extracellular parasites followed by drug selection to make stable transgenic lines expressing *Tg*FNT-HA proteins. The ensuing strains expressed *Tg*FNT1–3 under the control of *Tg*GRA1 elements targeted at the UPRT locus. Immunofluorescence studies revealed that all *Tg*FNTs were expressed at the surface of intracellular tachyzoites (Fig. 1*B*). Immunostaining of *Tg*FNT1–3 using an anti-HA antibody indicated a peripheral expression of all transporters, as judged by their colocalization with a *bona fide* marker of the inner membrane complex (*Tg*Gap45; Fig. S1*A*), located just underneath the parasite's plasma lemma (24). To determine the exact site of protein location, we treated extracellular parasites with bacterial α-toxin to split the plasma membrane from the inner membrane complex and performed co-staining of *Tg*FNT1–3 with a plasma membrane marker (*Tg*Sag1), and with *Tg*Gap45 (Fig. S1*A*). The HA signal overlapped clearly with *Tg*Sag1, but not with *Tg*Gap45, confirming the occurrence of all three *Tg*FNT-HA constructs at the parasite surface.

In further assays, we assessed the orientation of *Tg*FNT1–3 in the plasma membrane by immunostaining detergent-permeabilized and nonpermeabilized parasites (Fig. S1*B*). The

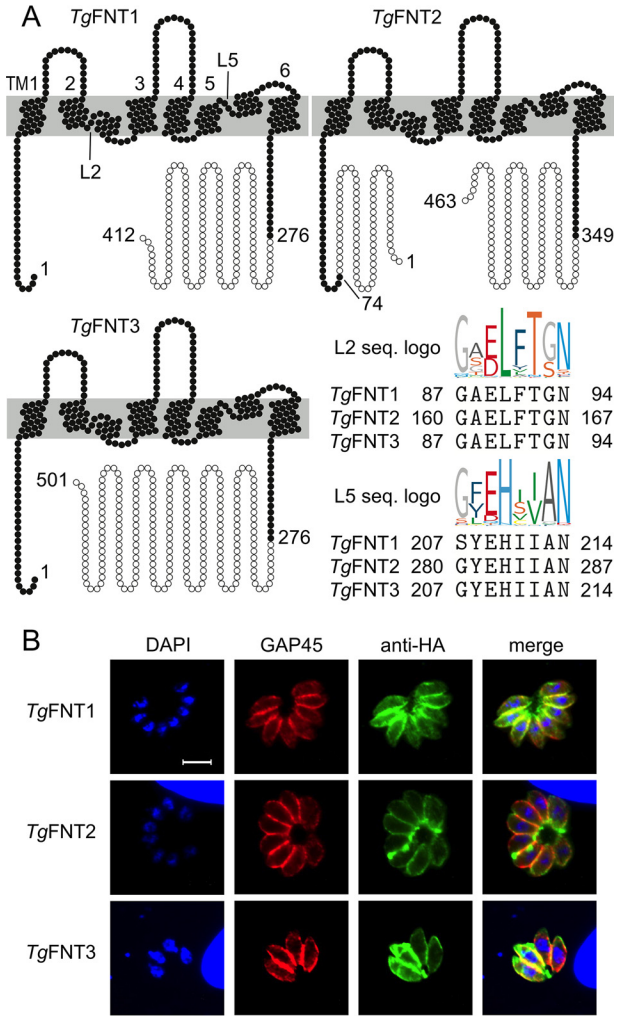

Figure 1. Topology plots and intracellular localization of *Tg*FNT1–3. *A*, shown is the six-transmembrane topology (TM1–6) and matching *Tg*FNT1–3 sequences (L2, L5) in two signature motifs of the FNT protein family (*logos*). *Open circles* indicate sequence sections that were truncated for expression of stable *Tg*FNT proteins in yeast. *B*, immunostaining of full-length *Tg*FNT1–3 constructs with a C-terminal HA epitope in intracellular tachyzoites of *T. gondii* (*green*). The tachyzoite nuclei (DAPI, *blue*) and inner membrane complex located just underneath the plasma membranes (GAP45, *red*) were counterstained. *Yellow color* in the merged images indicates the peripheral localization of the *Tg*FNT1–3. *Scale bar* = 5 μm.

presence of HA staining only in permeabilized parasites confirmed that the C termini of *Tg*FNT1–3 do face the cytosol, as predicted above (Fig. 1*A*). We also examined the endogenous expression profiles of these proteins based on the MS datasets in ToxoDB. Interestingly, only *Tg*FNT1 and *Tg*FNT2 are expressed at the protein level, whereas *Tg*FNT3 is not detectable in tachyzoites of the type I strain (*i.e.* RH strain used herein). The latter is however readily detectable in the cyst-forming type II strain (ME49 strain). These results together demonstrate the occurrence of three distinct FNTs located in the plasma membrane of *T. gondii*, of which only *Tg*FNT1 and *Tg*FNT2 are naturally expressed during the lytic cycle of the type I strain.

TgFNTs transport L-lactate as well as formate in a pH-dependent manner

To determine substrate specificity and kinetics of *Tg*FNT transport, we carried out biophysical import assays using radio-

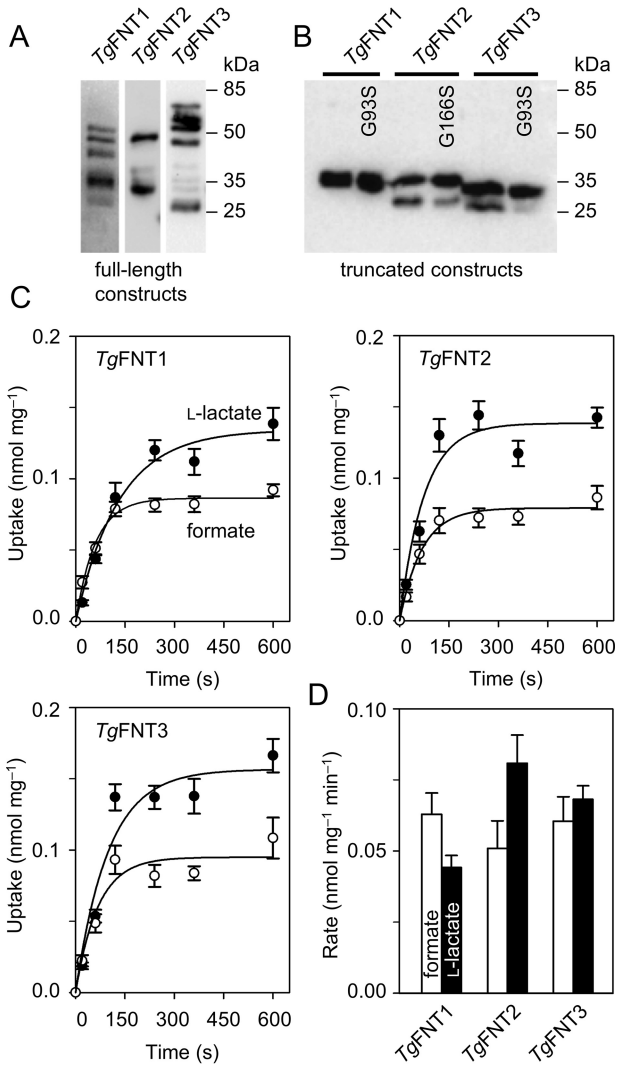

Figure 2. Expression of *Tg*FNT1–3 in yeast and determination of transport functionality. *A*, Western blotting of full-length *Tg*FNT1 (44.3 kDa), *Tg*FNT2 (50.8 kDa), and *Tg*FNT3 (53.3 kDa) detected via an N-terminal HA epitope revealing strong protein fragmentation. *B*, Western blotting of the truncated versions of *Tg*FNT1 (30.3 kDa), *Tg*FNT2 (29.9 kDa), and *Tg*FNT3 (30.0 kDa) as well as glycine-to-serine mutants showing improved protein stability. *C*, uptake of ^{14}C-labeled formate (*open circles*) and L-lactate (*closed circles*) by *Tg*FNT1–3 (pH 6.8, 1 mM inward gradients). Data were normalized to 1 mg of dried yeast after background subtraction from nonexpressing yeast. *D*, uptake rates of formate (*open bars*) and L-lactate (*closed bars*) derived from single exponential fittings of the uptake curves. *Error bars* indicate S.E. from three biological replicates, each with triplicate measurements.

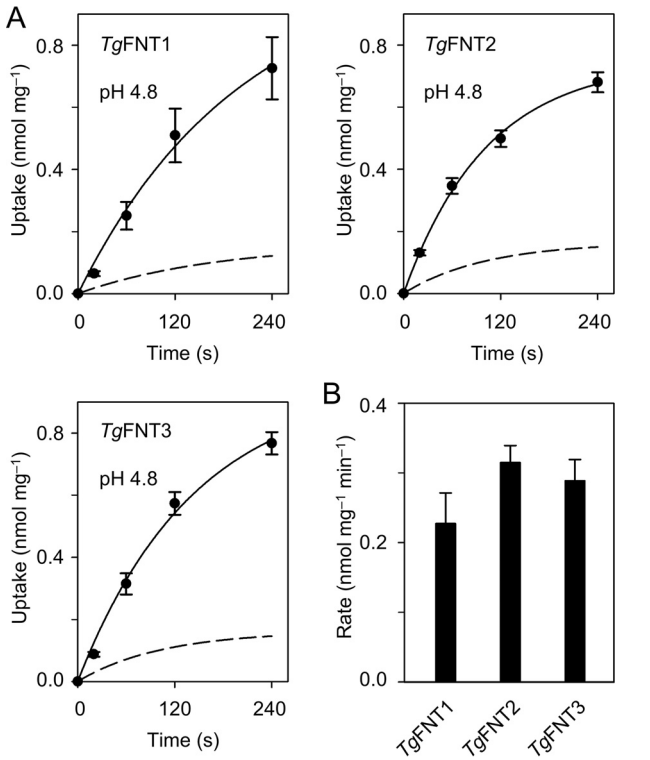

Figure 3. pH-dependent L-lactate transport of *Tg*FNT1–3 in yeast. *A*, shown is the L-lactate uptake at pH 4.8 compared with pH 6.8 (*dashed lines*; data from Fig. 2*C*). *B*, uptake rates of L-lactate as deduced by single exponential fittings of the uptake curves. Three independent assays were carried out, each with triplicate data points. *Error bars* denote S.E.

labeled formate and lactate in an established *Saccharomyces cerevisiae* strain (W303–1A *jen1*Δ *ady2*Δ) lacking endogenous monocarboxylate transporters (7, 8, 25). Transport was monitored over a short time scale (second to minute) to prohibit any metabolic and phenotypic effects. Under these conditions, uptake of radioisotope is directly linked to specific substrate transport via the recombinantly expressed *Tg*FNT. Others and we have shown before that FNT transport is bidirectional (6, 8). Initially, we expressed full-length ORFs of *Tg*FNT1–3. It turned out however that the resulting proteins were highly unstable in the yeast system, appearing as multiple fragments in immunoblots (Fig. 2*A*). Consequently, our import assays with ^{14}C-radiolabeled formate or L-lactate as substrates yielded erratic results. Earlier studies on the structure and transport mechanism of the FNTs suggested that despite a probably flexible N-terminal domain, the core protein assumes a rather rigid, channel-like conformation (25). Hence, we presumed that protein-stabilizing deletions in *Tg*FNTs might be tolerated without affecting their basic transport function and substrate selectivity. Indeed, shortening of the termini to the lengths indicated in Fig. 1*A* resulted in reasonably stable expression of all three transporters in yeast (Fig. 2*B*), which enabled a detailed functional characterization.

The truncated *Tg*FNT1–3 proteins were functional transporting formate and L-lactate. The three transporters produced similar substrate uptake curves for formate and L-lactate in 1 mM inward-directed gradients at pH 6.8 (Fig. 2*C*), which is comparable in magnitude to the FNT from *P. falciparum* (8). The initial import rates of all *Tg*FNTs, as determined by exponential fittings, indicated nearly equal preference for the formate molecule (45 Da) and for the twice as large L-lactate (89 Da) (Fig. 2*D*). In the steady state of transport, lactate accumulated at 50–60% higher levels in the yeast cells than formate. Earlier, we established that the transmembrane proton gradient is a driving force for monocarboxylate transport via FNT-type proteins (25). Accordingly, increasing acidity of the external buffer increases import rates of monocarboxylates. Hence, we monitored lactate import by *Tg*FNT1–3 at a lowered pH of 4.8, *i.e.* by two logarithmic units, which resulted in about 4-fold higher transport rates (Fig. 3, *A* and *B*). In summary, our data reveal the encoding of three functional FNT-type monocarboxylate/H^+ symporters in *T. gondii*.

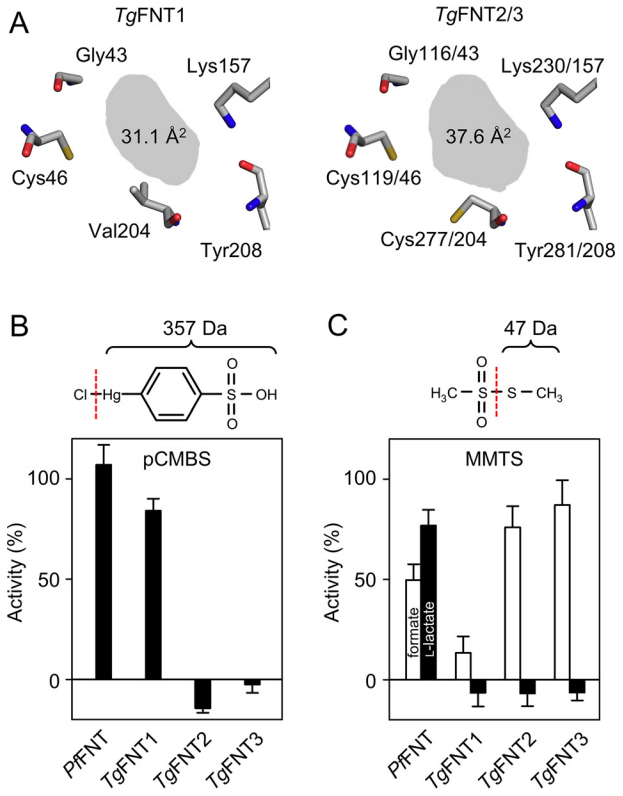

Figure 4. Identification of the *Tg*FNT1–3 Φ/K substrate selectivity filters and modulation by chemical cysteine modification. *A*, structure models of the selectivity filter layout (*top view*) and shading of the van der Waals section area (*gray*). *B*, effect of the organomercurial pCMBS (100 μM) on the L-lactate transport activity (pH 6.8, 1 mM inward gradient) of *P. falciparum* FNT (*Pf*FNT) and *Tg*FNT1–3 in yeast. The chemical structure and weight of the modifying entity (part right of the *dashed line*) is shown on the top. *C*, effect of cysteine-modification by MMTS (1 mM, structure and weight of transferred moiety *on top*) on formate (*open bars*) and L-lactate transport (*closed bars*) by *Pf*FNT and *Tg*FNT1–3 in yeast. *Error bars* are S.E. from three independent assays, each with triple measures.

The substrate selectivity filters in TgFNTs are wide

FNTs select substrates based on size exclusion in the Φ/K selectivity filter. The filter is composed of an invariant lysine side chain for monocarboxylate anion attraction, the backbone carbonyl oxygen of a neighboring amino acid, and the side chains of three further residues (Fig. 4*A*). The nature of the latter three amino acids determines the diameter of the filter (7). For instance, prokaryotic FNTs are characterized by large aromatic residues which narrow the filter and restrict passage to only small substrates, such as formate and nitrite. In contrast, the eukaryotic *Plasmodium* FNT, *Pf*FNT, carries short-chain amino acids allowing passage of larger substrates because of a resulting wider selectivity filter (7). We determined the composition of the selectivity filters in *Tg*FNT1–3 by sequence comparison (Fig. 4*A*). The filter layout of the three *Tg*FNTs is almost identical with only one variant, *i.e.* Val-204 in *Tg*FNT1 corresponding to Cys-277 and Cys-204 in *Tg*FNT2 and *Tg*FNT3, respectively. The highly similar filter regions offer an explanation for the observed similarities in the *Tg*FNT1–3 transport properties (Figs. 2 and 3). To confirm our structure prediction, we aimed at chemically modifying the indicated cysteine residues. At first, we added a cysteine-reactive, comparably large, aromatic organomercurial, 4-(chloromercuri)benzenesulfonate (pCMBS) to the *Tg*FNT assays (Fig. 4*B*). As a control, we tested *Pf*FNT, which is insensitive to pCMBS because of absence of cysteines in the transport path (8). Indeed, pCMBS fully inhibited *Tg*FNT2 and *Tg*FNT3, whereas *Tg*FNT1 remained entirely functional (Fig. 4*B*). The data imply that, unlike *Tg*FNT1, the filter regions in *Tg*FNT2 and *Tg*FNT3 expose pCMBS-accessible cysteines.

Assuming that pCMBS might be too voluminous to approach Cys-46 in *Tg*FNT1, we switched to a smaller cysteine-reactive compound, *i.e.* methyl methanethiosulfonate (MMTS), which transfers a thiomethyl moiety to cysteines forming a disulfide bridge (Fig. 4*C*). *Pf*FNT with a cysteine-less Φ/K filter was again included as a negative control. The observed slightly reduced transport rates of *Pf*FNT in the presence of MMTS are probably because of competition with the substrate, because MMTS is similar in size as formate and L-lactate, and was present at the same concentration. Notably however, MMTS treatment fully inhibited formate and lactate transport of *Tg*FNT1, showing that the cysteine modification can indeed block the selectivity filter (Fig. 4*C*). Remarkably, the effect of MMTS on *Tg*FNT2 and *Tg*FNT3 was rather distinguished: both excluded L-lactate yet allowed the formate to pass (Fig. 4*C*). Apparently, the modification by MMTS led to an intermediate filter diameter, which then exhibited the selectivity profile similar to the prokaryotic FNT proteins. Collectively, these experiments not only underline the mechanism of FNT functioning, but also reveal a divergent evolution of *Tg*FNT1–3, which likely serves special purposes during the natural life cycle of *T. gondii*.

Druglike inhibitors can block L-lactate transport by TgFNT1–3

Our earlier study has described druglike, high-affinity inhibitors of *Pf*FNT (26). By selection of a *Pf*FNT G107S resistance mutant, we located the drug-binding site to the intracellular substrate-entry region of *Pf*FNT. In this study, we chose the original screening hit compound from the *malaria box*, MMV007839, along with four other compounds with the same pharmacophore but different lipophilicity from our own collection for testing on *Tg*FNT1–3 (Fig. 5*A*). BH-296 lacks a phenolic hydroxyl moiety maintaining the molecule in the linear, active form, whereas BH-317, BH-326, and BH-388 can undergo the same repeated conversion between the active vinylogous acid form and a cyclic hemiketal form, as we showed before for MMV007839 (26). All compounds ablated L-lactate transport by *Tg*FNT1–3 (Fig. 5*B* and Fig. S2). Consistent with its deviant substrate selectivity filter, *Tg*FNT1 required double-digit micromolar concentrations for half-maximal inhibition, whereas *Tg*FNT2 and *Tg*FNT3 were more susceptible yielding IC_{50} values even in the nanomolar range (Table 1).

To test whether the binding site of the inhibitors to *Tg*FNT1–3 corresponds to *Pf*FNT, we introduced single mutations in *Tg*FNT1 (G93S), *Tg*FNT2 (G166S), and *Tg*FNT3 (G93S), mimicking the resistance mutation observed in the *Pf*FNT protein. The altered proteins were expressed in yeast at the same levels as the corresponding nonmutated variants (Fig. 2*B*), albeit the transport rates for lactate were reduced by about half (Fig. 6*A*). In each case, the glycine-to-serine mutation shifted the IC_{50} value of MMV007839 toward a higher value, *i.e.* 4× in *Tg*FNT1 G93S (108.0 ± 8.1 μM), 46× in *Tg*FNT2 G166S

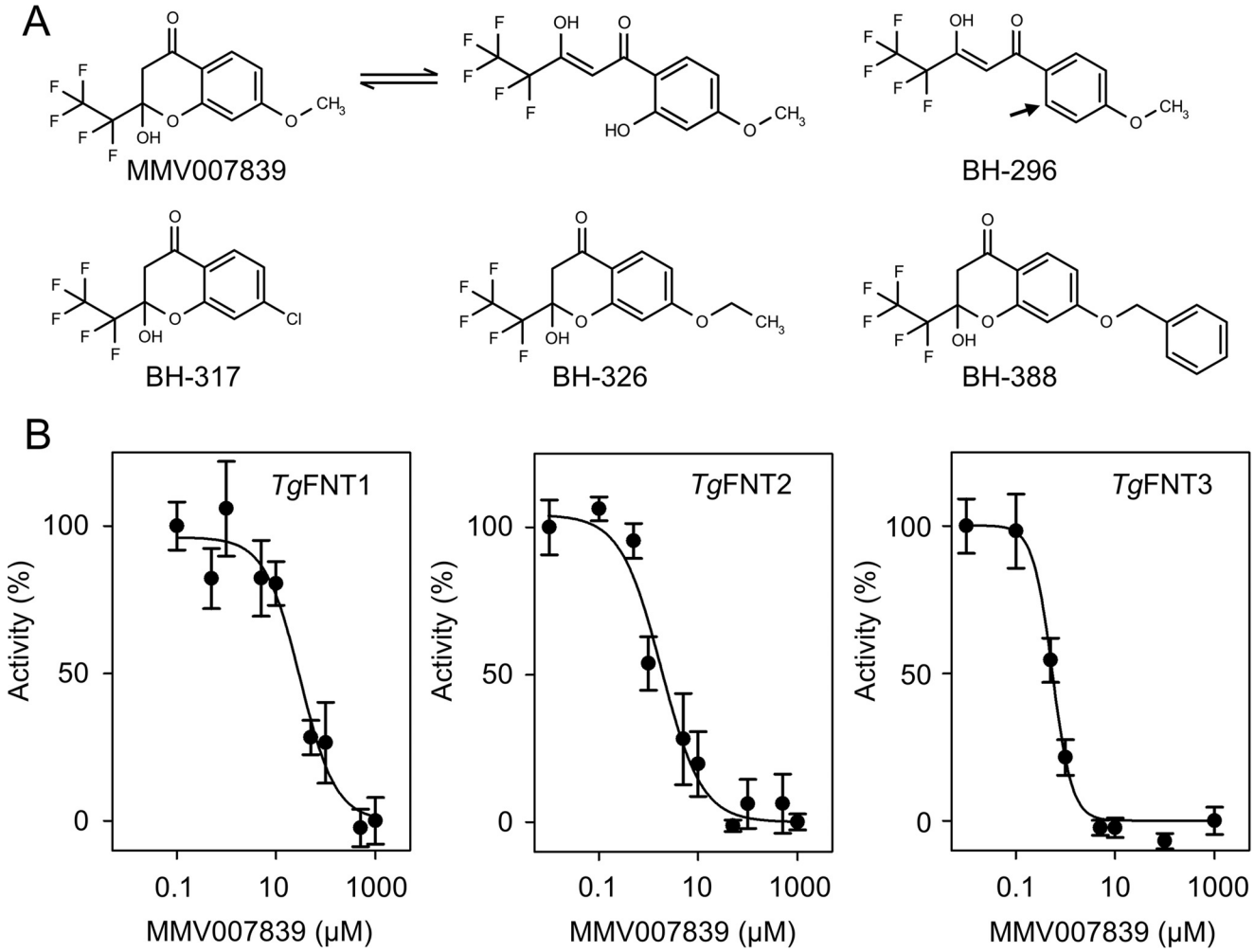

Figure 5. Inhibition of *Tg*FNT1–3 L-lactate transport by small molecules in yeast. *A*, the chemical structures of the compounds varying in their aromatic substituent. MMV007839, BH-317, BH-326, and BH-388 undergo repeated conversions between a cyclic hemiketal transport form and a linear vinylogous acid active form. BH-296 lacks a phenolic hydroxyl moiety (*arrow*) maintaining the molecule in the linear form. *B*, dose-dependent inhibition of *Tg*FNT1–3 by MMV007839 (pH 6.8, 1 mM inward gradient). Three biological assays were done, each with triplicate data points. *Error bars* denote S.E.

Table 1

Inhibitor efficiency on *Tg*FNT1–3 expressed in yeast and on tachyzoites in culture

	IC_{50} (μM)			
Inhibitors	*Tg*FNT1 (yeast)	*Tg*FNT2 (yeast)	*Tg*FNT3 (yeast)	Parasite growth
MMV007839	28.8 ± 10.5	1.94 ± 1.05	0.55 ± 0.08	47.1 ± 33.6
BH-296	56.0 ± 3.3	6.14 ± 4.59	3.00 ± 1.54	9.8 ± 1.8
BH-317	13.0 ± 2.4	0.92 ± 0.27	0.65 ± 0.08	15.8 ± 3.1
BH-326	22.3 ± 2.4	0.57 ± 0.13	0.59 ± 0.08	23.4 ± 8.2
BH-388	24.0 ± 3.0	4.78 ± 0.84	2.59 ± 0.08	5.8 ± 2.4

(88.8 ± 13.4 μM), and 149× in *Tg*FNT3 G93S (82.0 ± 7.9 μM) (Fig. 6*B*). Yet again, *Tg*FNT1 was quantitatively less susceptible to a mutation-driven change in the IC_{50} value.

Inhibition of TgFNT1–3 impairs the lytic cycle

To determine the anti-parasitic effect of the *Tg*FNT1–3 inhibitors, we set up plaque assays, which recapitulate the successive lytic cycles of tachyzoites, and thus the overall growth fitness of the parasite in cultures (27). To begin with, we analyzed concentrations of 1 μM and 10 μM for all compounds (Fig. 7*A*); higher concentrations were not tolerated by the host cells. The parasite growth appeared normal at 1 μM, but was differentially inhibited at 10 μM. As shown in Fig. 7*B*, BH-296 and BH-388 resulting in the smallest average plaque size, were most potent among all. Parasite growth was inhibited by about 35% in the presence of BH-296 and BH-388, whereas BH-312 and BH-326 exerted a modest 10% inhibition.

We also measured the replication rates in the presence of these chemicals using a strain that expresses the yellow fluorescent protein (YFP) in its cytosol (28). Because the YFP signal correlates with the replication rate of tachyzoites, it provides a rapid and accurate measurement of the parasite growth (Fig. 7*C*). Similar to the plaque assays, BH-296 and BH-388 were most effective against the parasite (Fig. 7*C*; Table 1), whereas the other three compounds were less active, as judged by a much higher IC_{50} of the growth inhibition (Fig. S3). Irrespective of their distinguishable IC_{50} values in the transport assays, the IC_{50} values of growth inhibition fall into a similar range. To conclude, these results suggest that FNT inhibitors can block the asexual reproduction of *T. gondii*, which resonates with our biochemical assays.

Discussion

Plasmodium and *Toxoplasma* are long known to be voracious consumers of glucose during their acute infection phase

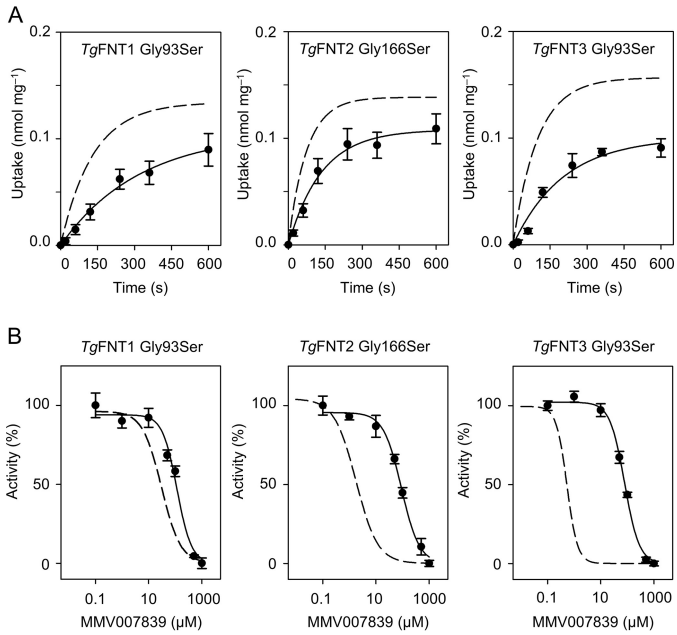

Figure 6. Functionality and inhibition of *Tg*FNT glycine-to-serine mutants in yeast. *A*, transport of L-lactate by the *Tg*FNT mutants (pH 6.8, 1 mM inward gradient) compared with the nonmutated proteins (*dashed lines*). *B*, glycine-to-serine mutations in *Tg*FNT1–3 shift the MMV007839 inhibition curves to higher concentrations (*dashed lines* represent the positions of curves with nonmutated *Tg*FNTs from Fig. 5*B*). The experiments were carried out three times, each in triplicates. *Error bars* denote S.E.

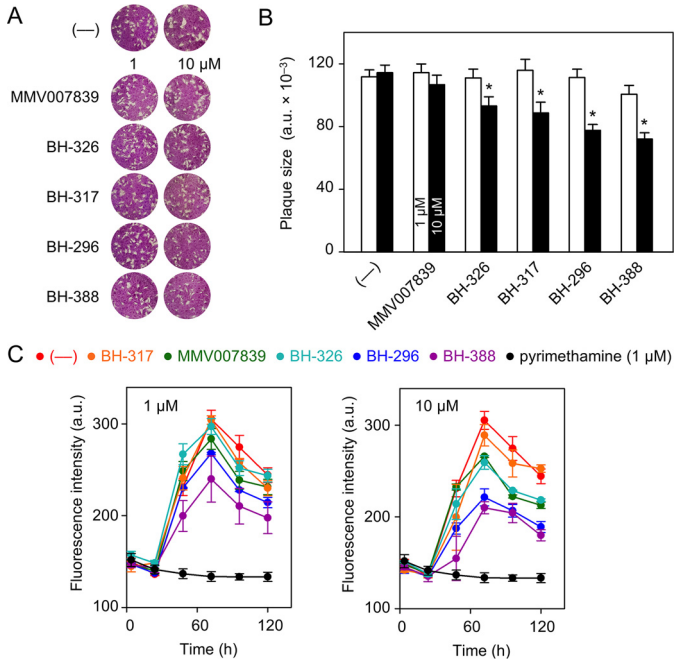

Figure 7. TgFNT inhibitors can impair the tachyzoite growth. *A*, overall growth fitness of tachyzoites, as judged by plaque assays. Plaques form after parasite-inflicted lysis in the host cell monolayer during the lytic cycles of tachyzoites. The plaque size correlates with the parasite fitness. Parasites were treated with the carrier solvent DMSO (—) or with *Tg*FNT inhibitors at 1 μM and 10 μM. *B*, plaque size determination by image analysis at 1 μM (*open bars*) and 10 μM (*closed bars*) inhibitor concentration. *Asterisks* label significant differences ($p < 0.05$; Student's *t* test). *C*, effect of *Tg*FNT inhibitors (100 μM, 10 μM, and 1 μM) on the parasite replication as determined by fluorescence intensity of YFP-expressing tachyzoites. The compound *color code* is indicated above the graphs. Pyrimethamine (1 μM in all plots) and DMSO-treated parasites (—) served as the positive and negative controls, respectively. The results show three independent assays, each done in triplicates (± S.E.).

(9–11). Glucose is catabolized primarily via glycolysis, resulting in a substantial production of L-lactate as a key by-product. Both parasites release the excess of L-lactate to the external milieu to sustain their proliferation. Previously, we have characterized *Pf*FNT, which is the sole L-lactate transporter expressed in *P. falciparum*. Herein, we show the presence of multiple FNT isoforms to perform the same task in tachyzoites of *T. gondii*. A functional link between glycolysis and FNT proteins is corroborated by concordant transcript profiles of *Tg*FNT1–3, the glucose transporter, and the enzymes of glycolysis during the lytic cycle of tachyzoites (Fig. S4). An apparent redundancy in L-lactate transport is also in accordance with the exceptional metabolic plasticity observed in the central carbon metabolism of tachyzoites (16, 18, 19). FNTs discriminate between different monocarboxylate substrates by size selection in the Φ/K filter region (7). In view of an almost identical filter layout of TgFNT1–3 the question arises why *T. gondii* expresses three isoforms. Besides mere redundancy, it is plausible that they serve different parasite stages during the natural life cycle. Glucose import is critical for *Plasmodium* species (17, 18), whereas *T. gondii* tachyzoites can survive without it, albeit with a modest growth defect (13, 16). In accord with *Pf*FNT, inhibition of the singular hexose transporter in *Plasmodium* (*Pf*HT) kills the parasite (17, 29), validating both *Pf*HT and *Pf*FNT as antimalarial targets. It is indeed surprising to see a lethal phenotype in tachyzoites upon inhibition of *Tg*FNTs in the micromolar range of these compounds. Notwithstanding putative off-target effects, the data suggest a critical role of lactate transport, which remains to be confirmed by gene knockout studies.

The pH-dependence of *Tg*FNT1–3 reported herein is comparable with *Pf*FNT (8), suggesting that both parasites employ the same mechanism to transport lactate. The underlying "dielectric slide" mechanism is based on the electrostatic attraction of the deprotonated substrate anion into the FNT vestibule and subsequent neutralization by protonation allowing for passage through two hydrophobic constriction sites in the protein (25, 30). Transport of the comparatively large L-lactate molecule via *Tg*FNT1–3 is facilitated by a substrate selectivity filter, which is wider than that of bacterial formate–nitrite transporters. The Φ/K selectivity filter with its size exclusion principle and the usual FNT fold are highly reminiscent of the aquaporin (AQP) water and solute channels (31, 32). Six transmembrane helices in conjunction with two half-helices fold into one transduction unit (Fig. 1*A*), which oligomerizes to form a homomeric FNT pentamer. AQPs with their distinct primary sequences form homotetramers, yet the FNT and AQP protomers can be superimposed with only small deviations (23). The access path from the extracellular side to the selectivity filter appears deeper in *Tg*FNT1 compared with pCMBS-sensitive AQPs that carry a respective cysteine residue (33). On the other hand, it is narrower compared with *Tg*FNT2 and *Tg*FNT3, because the organomercurial did not reach the cysteine at the filter site of *Tg*FNT1, leaving its functionality unaffected (Fig. 4*B*). In support of this notion, our structure models of *Tg*FNT2 and *Tg*FNT3 show a 20% larger section area in the Φ/K region than *Tg*FNT1 (Fig. 4*A*). Cysteine-modification by MMTS provides direct evidence for the difference in width

of the selectivity filters in *Tg*FNT1 and *Tg*FNT2/3 proteins. Whereas the former was blocked upon addition of a small thiomethyl moiety, the latter two tolerated the chemical modification, albeit with the restriction of smaller transport substrates.

Similarly, our inhibitor compounds, which block *Tg*FNT1–3 at the intracellular entrance of the transport path, were less efficient in accessing and binding *Tg*FNT1 than *Tg*FNT2 or *Tg*FNT3. As a result, the IC_{50} values turned out to be considerably higher for *Tg*FNT1. IC_{50} values obtained in the *in vitro* cultures of *T. gondii* tachyzoites were in a similar range with *Tg*FNT1 expressed in yeast, suggesting it to be the major target of inhibitors used here. However, it should be noted that the compounds must enter the parasite cytosol to reach the *Tg*FNT-binding site. This requires the inhibitors to pass the plasma membranes of the host cell and parasites by diffusion or active transport. Further, the compounds must exhibit a certain metabolic stability inside the cells to maintain their chemical structure for binding to the *Tg*FNTs. Our prior observations in the *Plasmodium* system show that even small structural differences of the inhibitor compounds, *e.g.* the presence or absence of a methoxy moiety, can have major effects on their potency in the *in vitro* parasite culture despite an equal activity in the yeast system (26). Therefore, phenotypic drug screenings should stand a better chance to identify compounds with good efficiency against living parasites than assays with isolated target proteins.

In summary, this study has identified and characterized the previously unknown lactate transporters of *T. gondii*. Moreover, we showed that blockers of *Tg*FNTs can inhibit the parasite growth, rendering them potential novel drug targets. The work advocates further studies on the comparative metabolic importance of three *Tg*FNT isoforms.

Experimental procedures

DNA sequences and protein analysis

DNA and protein sequences were derived from ToxoDB and the NCBI databases. Protein structure data were derived from RCSB data bank. Sequence alignments and logos were set using TeXshade and TeXtopo (34, 35). *Tg*FNT structure models were generated with SWISS-MODEL (36) using *S. typhimurium* FocA (PDB ID: 3Q7K) (37) as a template. Visualization of protein structures was done using the PyMOL Molecular Graphics System, Schrödinger, LLC.

Expression of TgFNT1–3 in yeast

The ORF sequences of *Tg*FNT1 (TGGT1_209800), *Tg*FNT2 (TGGT1_292110), and *Tg*FNT3 (TGGT1_229170) were codon-optimized, synthesized (GenScript), and cloned into the yeast expression vector pDR196 using SpeI and SalI (*Tg*FNT1) or SpeI and XhoI (*Tg*FNT2, *Tg*FNT3). The pDR196 vector encodes an N-terminal hemagglutinin epitope and a C-terminal His_{10} tag. The truncated *Tg*FNT versions were generated by PCR using the primers (Life Technologies) indicated in Table S1 and cloned into the WT constructs. Point mutations were introduced by site-directed mutagenesis using the QuikChange protocol (Stratagene) (primers with the respective nucleotide exchanges are shown in Table S1). All constructs were sequenced for accuracy prior to further use. Transformation of W303-1A *jen1*Δ *ady2*Δ (MATa, can1-100, ade2-loc, his3-11-15, leu2-3,-112, trp1-1-1, ura3-1, jen1::kanMX4, ady2::hphMX4) yeast cells, kindly provided by M. Casal (38), was done using the lithium acetate/single stranded carrier DNA/PEG procedure (39). Transformed cells were grown at 30 °C in selective media (S.D.) containing adenine, histidine, leucine, tryptophan, and 2% (w/v) glucose in the absence of uracil.

Western blotting

A 100 ml yeast liquid culture in selective media (S.D.) was prepared and cells were collected at an A_{600} of 1 (1000 *g*, 5 min, 4 °C), washed with 25 ml water and 10 ml extraction buffer (5 mM EDTA, 25 mM Tris, pH 7.5), pelleted, and resuspended in 0.5 ml of extraction buffer. Cells were disrupted by adding 0.5 g acid-washed glass beads (diameter 0.5 mm; Sigma-Aldrich) followed by 10 cycles of vortexing (30 s each) and intermittent cooling on ice for 1 min. Cell lysates were cleared (1000 × *g*, 5 min, 4 °C) and the membrane fraction was collected at 10,000 × *g* for 5 min at 4 °C. The pellet was resuspended in 0.1 ml of 100 mM phosphate buffer, pH 8.0, with 50 mM NaCl. Proteins were separated by SDS-PAGE and blotted on PVDF membranes (Hybond-P, Amersham Bioscience). Detection was done with a monoclonal mouse anti-hemagglutinin antibody (Roche) and a horseradish peroxidase–conjugated secondary antibody (Jackson ImmunoResearch Laboratories) using the ECL Plus system (GE Healthcare) for chemiluminescence (Lumi-Imager F1, Roche).

TgFNT1–3 transport assays in yeast

Assays were done as described earlier (8). Briefly, a yeast liquid culture in selective media (S.D.) was harvested at an A_{600} of 1, and the cells were resuspended in 50 mM HEPES/Tris buffer (pH 6.8), or in 50 mM citric acid/Tris buffer (pH 4.8). The yeast cell suspensions were adjusted to an A_{600} of 50 (±10%) and kept on ice. The transport assays were started by adding 20 μl of the substrate solution to 80 μl of yeast suspension to yield a final concentration of 1 mM substrate and 0.04 μCi radiolabeled [1-^{14}C] substrate (formate or L-lactate). Assays were done at 18 °C. Substrate uptake was stopped at specified time points by abrupt dilution with 1 ml ice-cold water and rapid transfer onto a vacuum filtration unit fitted with a GF/C filter membrane (Whatman). After washing with 7 ml ice-cold water, the filter membranes were transferred into scintillation vials filled with 3 ml of scintillation fluid (Quicksafe A, Zinsser Analytic). Vials were analyzed using a liquid scintillation counter (Packard Tri-Carb, PerkinElmer Life Sciences). The transport rates were calculated from single-exponential fittings. Unless specified otherwise, all assays were performed with three independent biological replicates. The background subtraction was done using the nonexpressing parental yeast cells. The given S.E. error margins can be converted into standard deviation by multiplication with the square root of 3, *i.e.* 1.732.

Chemical modification and inhibition of TgFNTs in yeast

80 μl of yeast cell suspension were incubated with 100 μM pCMBS or 1 mM MMTS for 30 min at 18 °C. The transport assays were stopped at 2 min, *i.e.* in the initial linear uptake phase. For determination of IC_{50} values, 1 μl of DMSO with or

without test compound at different concentrations was added to 80 μl of the cell suspension 15–20 min prior to the assay solution. Uptake was stopped in the initial linear phase, *i.e.* at 2 min for truncated WT *Tg*FNT1–3, and at 4 min for the Gly to Ser mutants, respectively. Three independent assays, each in triplicate was done.

Parasite culture

Tachyzoites of *T. gondii* (RH-hxgprt$^-$ and RH-hxgprt$^-$–YFP strain) were cultured in confluent monolayers of primary human foreskin fibroblast (HFF) cells, essentially as described before (28, 40). Briefly, the host cells were maintained in DMEM supplemented with fetal bovine serum (10%), glutamine (2 mM), sodium pyruvate (1 mM), penicillin (100 units ml^{-1}), streptomycin (100 μg ml^{-1}), and 1× nonessential amino acids (minimum Eagle's medium). Cultures were incubated at 37 °C in a humidified incubator with 5% CO_2. For regular parasite cultures, HFF cells were infected with a multiplicity of infection of 3, and tachyzoites were passaged every second day into fresh host cells.

Expression of TgFNT1–3 in tachyzoites

The full-length ORFs of *Tg*FNT1–3 were cloned into *pGRA1-UPKO* vector digested with *Nsi* I/*Pac* I sites. The forward primer for *Tg*FNT1 contained *Sbf* I (compatible with *Nsi* I in the vector), whereas the forward primers of *Tg*FNT2–3 were engineered with *Nsi* I sites (Table S1). The reverse primers for all ORFs contained *Pac* I sites. This vector allowed stable genomic insertion of the single-copy *Tg*FNT1–3 expression cassettes at the uracil phosphoribosyltransferase locus via negative selection with 5-fluorodeoxyuridine (FUdR) (41). To make transgenic strains, fresh extracellular tachyzoites (~10^7) were harvested and suspended in cytomix buffer (120 mM KCl, 0.15 mM $CaCl_2$, 10 mM K_2HPO_4/KH_2PO_4, 25 mM HEPES, 2 mM EGTA, 5 mM $MgCl_2$, 5 mM GSH, 5 mM ATP) and 10 μg plasmid, immediately followed by electroporation (BTX instruments). Transfected tachyzoites were used to infect confluent host cells and drug-selected with 5-fluorodeoxyuridine before subjecting them to immunolocalization assays.

Indirect immunofluorescence assays

HFF cells seeded on glass coverslips were infected with freshly isolated tachyzoites for 24 h, fixed with 4% paraformaldehyde for 10 min, and then neutralized with 0.1 M glycine in PBS for 5 min. Samples were permeabilized by 0.1% Triton X-100 in PBS for 20 min, blocked with 2% BSA in PBS/0.1% Triton X-100 for 20 min. Subsequently, they were stained with primary antibodies (mouse anti-HA, 1:10,000; rabbit anti-*Tg*-Gap45, 1:10,000) for 1 h and then with respective secondary antibodies (Alexa Fluor 488 and Alexa Fluor 594, 1:3000) for 45 min in the dark. Samples were mounted into a mix of Fluoromount-G and DAPI, dried at 4 °C overnight and examined by fluorescence microscopy (ApoTome, Zeiss). To resolve the C-terminal topology of *Tg*FNT1–3, extracellular parasites were stained with a mouse α-HA antibody (1:3000), suspended either in 3% BSA/PBS solution for pre-permeabilization staining, or in 2% BSA/0.2% Triton X-100/PBS for post-permeabilization, as shown in Fig. S1. The inner membrane complex was separated from the plasma membrane by treating extracellular parasites with α-toxin from *Clostridium septicum* (20 nM, 2 h) (List Biological Laboratories) followed by fixation on BSA-coated (0.01%) coverslips. In both cases, the standard secondary antibody staining procedure was performed afterward, as described above.

Parasite growth assays

Plaque assays were done in 6-well plates seeded with HFF cells (42). Inhibitors were dissolved in DMSO, and then mixed with 2 ml of culture media before diluting them to desired amounts into each well. The carrier solvent DMSO was also included as a control alongside in all assays. Host cell monolayers were infected with 150 parasites, and parasitized cells were cultured unperturbed for 7 days (37 °C, 5% CO_2). Samples were fixed with ice-cold methanol for 10 min and then stained with crystal violet dye for 15 min. The plaque sizes were measured using the ImageJ program (National Institutes of Health). To set up YFP-based growth assays, HFF monolayers in 96-well plates were infected with 7 × 10^3 tachyzoites of the RH-hxgprt$^-$–YFP strain. After 4 h, the inoculation medium was replaced by colorless medium (free of phenol red) containing 1, 10, or 100 μM of the indicated compounds. The YFP fluorescence intensity was recorded every 24 h for up to 120 h (excitation, 485 nm; emission, 528 nm; area scan mode). Parasites treated with 1 μM pyrimethamine or with DMSO served as the positive and negative controls, respectively.

Author contributions—H. E., B. R., N. G., and E. B. validation; H. E., B. R., N. G., and E. B. investigation; H. E., B. R., and E. B. visualization; H. E., B. R., N. G., and E. B. methodology; H. E. and B. R. writing-review and editing; N. G. and E. B. conceptualization; N. G. and E. B. writing-original draft; E. B. formal analysis; E. B. supervision; E. B. funding acquisition; E. B. project administration.

Acknowledgments—We thank B. Henke and A. Fuchs for technical assistance as well as M. Casal for providing the yeast strain (W303–1A jen1Δ ady2Δ).

References

1. Suppmann, B., and Sawers, G. (1994) Isolation and characterization of hypophosphite-resistant mutants of *Escherichia coli*: Identification of the FocA protein, encoded by the pfl operon, as a putative formate transporter. *Mol. Microbiol.* **11,** 965–982 CrossRef Medline
2. Jia, W., Tovell, N., Clegg, S., Trimmer, M., and Cole, J. (2009) A single channel for nitrate uptake, nitrite export and nitrite uptake by *Escherichia coli* NarU and a role for NirC in nitrite export and uptake. *Biochem. J.* **417,** 297–304 CrossRef Medline
3. Czyzewski, B. K., and Wang, D.-N. (2012) Identification and characterization of a bacterial hydrosulphide ion channel. *Nature* **483,** 494–497 CrossRef Medline
4. Beyer, L., Doberenz, C., Falke, D., Hunger, D., Suppmann, B., and Sawers, R. G. (2013) Coordination of FocA and pyruvate formate-lyase synthesis in *Escherichia coli* demonstrates preferential translocation of formate over other mixed-acid fermentation products. *J. Bacteriol.* **195,** 1428–1435 CrossRef Medline
5. Das, P., Lahiri, A., Lahiri, A., and Chakravortty, D. (2009) Novel role of the nitrite transporter NirC in *Salmonella* pathogenesis: SPI2-dependent suppression of inducible nitric oxide synthase in activated macrophages. *Microbiology* **155,** 2476–2489 CrossRef Medline

6. Marchetti, R. V., Lehane, A. M., Shafik, S. H., Winterberg, M., Martin, R. E., and Kirk, K. (2015) A lactate and formate transporter in the intraerythrocytic malaria parasite, *Plasmodium falciparum*. *Nat. Commun.* **6,** 6721 CrossRef Medline
7. Wiechert, M., Erler, H., Golldack, A., and Beitz, E. (2017) A widened substrate selectivity filter of eukaryotic formate-nitrite transporters enables high-level lactate conductance. *FEBS J.* **284,** 2663–2673 CrossRef Medline
8. Wu, B., Rambow, J., Bock, S., Holm-Bertelsen, J., Wiechert, M., Soares, A. B., Spielmann, T., and Beitz, E. (2015) Identity of a *Plasmodium* lactate/H^+ symporter structurally unrelated to human transporters. *Nat. Commun.* **6,** 6284 CrossRef Medline
9. McKee, R. W., Ormsbee, R. A., Anfinsen, C. B., Geiman, Q. M., and Ball, E. G. (1946) Studies on malarial parasites: VI. The chemistry and metabolism of normal and parasitized (*P. knowlesi*) monkey blood. *J. Exp. Med.* **84,** 569–582 CrossRef Medline
10. Shakespeare, P. G., and Trigg, P. I. (1973) Glucose catabolism by the simian malaria parasite *Plasmodium knowlesi*. *Nature* **241,** 538–540 Medline
11. Ohsaka, A., Yoshikawa, K., and Hagiwara, T. (1982) ^{1}H-NMR spectroscopic study of aerobic glucose metabolism in *Toxoplasma gondii* harvested from the peritoneal exudate of experimentally infected mice. *Physiol. Chem. Phys.* **14,** 381–384 Medline
12. Woodrow, C. J., Penny, J. I., and Krishna, S. (1999) Intraerythrocytic *Plasmodium falciparum* expresses a high affinity facilitative hexose transporter. *J. Biol. Chem.* **274,** 7272–7277 CrossRef Medline
13. Blume, M., Rodriguez-Contreras, D., Landfear, S., Fleige, T., Soldati-Favre, D., Lucius, R., and Gupta, N. (2009) Host-derived glucose and its transporter in the obligate intracellular pathogen *Toxoplasma gondii* are dispensable by glutaminolysis. *Proc. Natl. Acad. Sci. U.S.A.* **106,** 12998–13003 CrossRef Medline
14. MacRae, J. I., Dixon, M. W., Dearnley, M. K., Chua, H. H., Chambers, J. M., Kenny, S., Bottova, I., Tilley, L., and McConville, M. J. (2013) Mitochondrial metabolism of sexual and asexual blood stages of the malaria parasite *Plasmodium falciparum*. *BMC Biol.* **11,** 67 CrossRef Medline
15. Blume, M., Nitzsche, R., Sternberg, U., Gerlic, M., Masters, S. L., Gupta, N., and McConville, M. J. (2015) A *Toxoplasma gondii* gluconeogenic enzyme contributes to robust central carbon metabolism and is essential for replication and virulence. *Cell Host Microbe* **18,** 210–220 CrossRef Medline
16. Nitzsche, R., Zagoriy, V., Lucius, R., and Gupta, N. (2016) Metabolic cooperation of glucose and glutamine is essential for the lytic cycle of obligate intracellular parasite *Toxoplasma gondii*. *J. Biol. Chem.* **291,** 126–141 CrossRef Medline
17. Slavic, K., Straschil, U., Reininger, L., Doerig, C., Morin, C., Tewari, R., and Krishna, S. (2010) Life cycle studies of the hexose transporter of *Plasmodium* species and genetic validation of their essentiality. *Mol. Microbiol.* **75,** 1402–1413 CrossRef Medline
18. Blume, M., Hliscs, M., Rodriguez-Contreras, D., Sanchez, M., Landfear, S., Lucius, R., Matuschewski, K., and Gupta, N. (2011) A constitutive panhexose permease for the *Plasmodium* life cycle and transgenic models for screening of antimalarial sugar analogs. *FASEB J.* **25,** 1218–1229 CrossRef Medline
19. Nitzsche, R., Günay-Esiyok, Ö., Tischer, M., Zagoriy, V., and Gupta, N. (2017) A plant/fungal-type phosphoenolpyruvate carboxykinase located in the parasite mitochondrion ensures glucose-independent survival of *Toxoplasma gondii*. *J. Biol. Chem.* **292,** 15225–15239 CrossRef Medline
20. Bzik, D. J., Fox, B. A., and Gonyer, K. (1993) Expression of *Plasmodium falciparum* lactate dehydrogenase in *Escherichia coli*. *Mol. Biochem. Parasitol.* **59,** 155–166 CrossRef Medline
21. Xia, N., Yang, J., Ye, S., Zhang, L., Zhou, Y., Zhao, J., David Sibley, L., and Shen, B. (2018) Functional analysis of *Toxoplasma* lactate dehydrogenases suggests critical roles of lactate fermentation for parasite growth *in vivo*. *Cell. Microbiol.* **20,** e12794 CrossRef Medline
22. Garcia, C. K., Goldstein, J. L., Pathak, R. K., Anderson, R. G., and Brown, M. S. (1994) Molecular characterization of a membrane transporter for lactate, pyruvate, and other monocarboxylates: Implications for the Cori cycle. *Cell* **76,** 865–873 CrossRef Medline
23. Wang, Y., Huang, Y., Wang, J., Cheng, C., Huang, W., Lu, P., Xu, Y.-N., Wang, P., Yan, N., and Shi, Y. (2009) Structure of the formate transporter FocA reveals a pentameric aquaporin-like channel. *Nature* **462,** 467–472 CrossRef Medline
24. Frénal, K., Polonais, V., Marq, J. B., Stratmann, R., Limenitakis, J., and Soldati-Favre, D. (2010) Functional dissection of the apicomplexan glideosome molecular architecture. *Cell Host Microbe* **8,** 343–357 CrossRef Medline
25. Wiechert, M., and Beitz, E. (2017) Mechanism of formate-nitrite transporters by dielectric shift of substrate acidity. *EMBO J.* **36,** 949–958 CrossRef Medline
26. Golldack, A., Henke, B., Bergmann, B., Wiechert, M., Erler, H., Blancke Soares, A., Spielmann, T., and Beitz, E. (2017) Substrate-analogous inhibitors exert antimalarial action by targeting the *Plasmodium* lactate transporter PfFNT at nanomolar scale. *PLoS Pathog.* **13,** e1006172 CrossRef Medline
27. Arroyo-Olarte, R. D., Brouwers, J. F., Kuchipudi, A., Helms, J. B., Biswas, A., Dunay, I. R., Lucius, R., and Gupta, N. (2015) Phosphatidylthreonine and lipid-mediated control of parasite virulence. *PLoS Biol.* **13,** e1002288 CrossRef Medline
28. Gubbels, M. J., Li, C., and Striepen, B. (2003) High-throughput growth assay for *Toxoplasma gondii* using yellow fluorescent protein. *Antimicrob. Agents Chemother.* **47,** 309–316 CrossRef Medline
29. Joet, T., Eckstein-Ludwig, U., Morin, C., and Krishna, S. (2003) Validation of the hexose transporter of *Plasmodium falciparum* as a novel drug target. *Proc. Natl. Acad. Sci. U.S.A.* **100,** 7476–7479 CrossRef Medline
30. Wiechert, M., and Beitz, E. (2017) Formate-nitrite transporters: monoacids ride the dielectric slide. *Channels* **11,** 365–367 CrossRef Medline
31. Beitz, E., Wu, B., Holm, L. M., Schultz, J. E., and Zeuthen, T. (2006) Point mutations in the aromatic/arginine region in aquaporin 1 allow passage of urea, glycerol, ammonia and protons. *Proc. Natl. Acad. Sci. U.S.A.* **103,** 269–274 CrossRef Medline
32. Wree, D., Wu, B., Zeuthen, T., and Beitz, E. (2011) Requirement for asparagine in the aquaporin NPA signature motifs for cation exclusion. *FEBS J.* **278,** 740–748 CrossRef Medline
33. Murata, K., Mitsuoka, K., Hirai, T., Walz, T., Agre, P., Heymann, J. B., Engel, A., and Fujiyoshi, Y. (2000) Structural determinants of water permeation through aquaporin-1. *Nature* **407,** 599–605 CrossRef Medline
34. Beitz, E. (2000) TeXshade: Shading and labeling of multiple sequence alignments using LaTeX2e. *Bioinformatics* **16,** 135–139 CrossRef
35. Beitz, E. (2000) TeXtopo: Shaded membrane protein topology plots in LaTeX2e. *Bioinformatics* **16,** 1050–1051 CrossRef Medline
36. Biasini, M., Bienert, S., Waterhouse, A., Arnold, K., Studer, G., Schmidt, T., Kiefer, F., Gallo Cassarino, T., Bertoni, M., Bordoli, L., and Schwede, T. (2014) SWISS-MODEL: Modelling protein tertiary and quaternary structure using evolutionary information. *Nucleic Acids Res.* **42,** W252–W258 CrossRef Medline
37. Lü, W., Du, J., Wacker, T., Gerbig-Smentek, E., Andrade, S. L. A., and Einsle, O. (2011) pH-dependent gating in a FocA formate channel. *Science* **332,** 352–354 CrossRef Medline
38. Soares-Silva, I., Paiva, S., Diallinas, G., and Casal, M. (2007) The conserved sequence NXXS/THXS/TQDXXXT of the lactate/pyruvate:H^+ symporter subfamily defines the function of the substrate translocation pathway. *Mol. Membr. Biol.* **24,** 464–474 CrossRef Medline
39. Gietz, R. D., Schiestl, R. H., Willems, A. R., and Woods, R. A. (1995) Studies on the transformation of intact yeast cells by the LiAc/SS-DNA/PEG procedure. *Yeast* **11,** 355–360 CrossRef Medline
40. Gupta, N., Zahn, M. M., Coppens, I., Joiner, K. A., and Voelker, D. R. (2005) Selective disruption of phosphatidylcholine metabolism of the intracellular parasite *Toxoplasma gondii* arrests its growth. *J. Biol. Chem.* **280,** 16345–16353 CrossRef Medline
41. Donald, R. G., and Roos, D. S. (1995) Insertional mutagenesis and marker rescue in a protozoan parasite: Cloning of the uracil phosphoribosyltransferase locus from *Toxoplasma gondii*. *Proc. Natl. Acad. Sci. U.S.A.* **92,** 5749–5753 CrossRef Medline
42. Hartmann, A., Hellmund, M., Lucius, R., Voelker, D. R., and Gupta, N. (2014) Phosphatidylethanolamine synthesis in the parasite mitochondrion is required for efficient growth but dispensable for survival of *Toxoplasma gondii*. *J. Biol. Chem.* **289,** 6809–6824 CrossRef Medline